ADAPTIVE ENERGY COMPENSATION FOR FULL WAVEFORM INVERSION BASED ON SEISMIC ILLUMINATION ANALYSIS

HONGYU SUN[1], LIGUO HAN[1], JINGYI CHEN[2] and MIAO HAN[3]

[1] *College of Geo-exploration Science and Technology, Jilin University, Changchun, Jilin 130026, P.R. China. sunhongyu2014@foxmail.com, hanliguo@jlu.edu.cn*
[2] *Department of Geosciences, The University of Tulsa, Tulsa, OK 74104, U.S.A. jingyi-chen@utulsa.edu*
[3] *Oil & Gas Survey of China Geological Survey, Beijing 100029, P.R. China. 370441419@qq.com*

(Received September 29, 2015; revised version accepted February 15, 2016)

ABSTRACT

Sun, H., Han, L., Chen, J. and Han, M., 2016. Adaptive energy compensation for full waveform inversion based on seismic illumination analysis. *Journal of Seismic Exploration*, 25: 269-284.

Full waveform inversion (FWI) which is an advanced seismic imaging technique based on the data fitting of full wavefield simulation has become extremely important in both academic research and commercial application in recent years. During the implementation of FWI, seismic velocities of deeper and complex parts of the model cannot be well updated due to the weak energy of seismic wavefields where they have less contributions to the mismatch between observed and calculated data in the objective function, even though the large velocity contrasts do. The uneven distribution of energy may have a significantly negative effect on reconstructing velocity structures of deep and complex zones. Therefore, an adaptive energy compensation method based on seismic illumination analysis is proposed to improve the imaging quality for FWI. We discuss the effects of limited maximum offset and complex velocity structures on the inhomogeneous energy distribution of seismic wavefields in terms of 2D acoustic wave equation. Two-way seismic illumination analysis is applied to calculate wavefield energy, adaptively compensate and balance the gradients according to the reflection and transmission coefficients which represent the partitioning of seismic waves energy at an interface. Numerical examples demonstrate the improved imaging accuracy without sacrificing too much computational efficiency of FWI when the maximum is limited.

KEY WORDS: full waveform inversion, maximum offset, seismic illumination, reflection and transmission coefficients, adaptive energy compensation.

0963-0651/16/$5.00 © 2016 Geophysical Press Ltd.

INTRODUCTION

The estimation of seismic velocities has considerable influence on final imaging of the subsurface structure. Compared with the traditional seismic ray tracing and tomographic imaging, full waveform inversion (FWI) is an appealing method to obtain accurate subsurface imaging, which exploits the full information of pre-stack seismic data (Virieux and Operto, 2009). Over the last few decades, FWI has been developed in time domain (Tarantola, 1984; Son et al., 2013), frequency domain (Pratt et al., 1998, 1999; Brossier et al., 2009), Laplace domain (Shin et al., 2008, 2010) and even time-frequency hybrid domain (Sirgue et al., 2008; Xu and McMechan, 2014). Many strategies such as frequency selection (Sirgue and Pratt, 2004), multiscale inversion (Bunks et al., 1995; Boonyasiriwat et al., 2009; Fichtner et al., 2013) and high performance computing (Mao et al., 2012) have been used to improve the accuracy and efficiency of FWI. 3D FWI (Warner et al., 2013; Shin et al., 2014) and multi-parameter FWI (Alkhalifah, 2014, 2015) have been well developed recently. In addition, FWI has been successfully applied to real field data to build velocity models (Butzer et al., 2013; Vigh et al., 2014; Borisov et al., 2015). However, the conventional FWI methods have difficulty in reconstructing the deeper part of the velocity model due to the restricted maximum offset. Long-offset seismic acquisition not only records diving waves with vital low frequency data to recover the long wavelength components of velocity model but also provides adequate full wavefield information for FWI to construct the deeper targets. But the maximum offset is usually limited because of the high seismic acquisition costs. To invert the deep velocity structures, the reflection FWI (RFWI) (Xu et al., 2012a, 2012b; Chi et al., 2015) and layer stripping methods (Wang and Rao, 2009) were developed by considering reflection energy and weighed updating. To use the kinematic information of reflected waves, a migration/demigration process was used in RFWI, which will increase computational cost. The cost of layer stripping is also proportional to artificial divisions of layers. In the following, we will introduce an illumination factor as a weighting function to precondition the gradients of FWI in order to improve the image quality for the deeper velocity structures.

Seismic illumination analysis is used to describe the detecting capability of a specific acquisition system to subsurface targets based on a given velocity model (Xie et al., 2013). Wave equation illumination methods which avoid high-frequency and asymptotic approximations used in seismic ray tracing can be applied to complex media with strong velocity variations to obtain accurate illumination results. Studying seismic illumination can optimize acquisition parameters and save the cost of the field survey (Xie et al., 2013). Bian et al. (2015) optimized multi-vertical-cable acquisition system through target oriented illumination analysis in multiscale FWI to obtain high fidelity subsurface models. Moreover, Yang et al. (2013) demonstrated an illumination

compensation strategy for wavefield tomography in the image domain. As the uneven illumination intensity in the complex medium can affect the quality of migration and the stability of inversion, Zhou et al. (2015) applied wave equation illumination analysis to migration optimization. In this paper, we would like to focus on the effect of illumination on inversion and imaging, and ignore its function on the seismic survey optimization.

It is difficult for waveform inversion to recover the velocity variation in deeper part of the complex velocity model due to the uneven distribution of seismic energy. There are number of causes. First, the seismic reflected and refracted energy from deep zone is much weaker than that from shallow zone, especially in the case of the acquisition geometry with limited maximum offset. Second, the illumination blind areas caused by complex geological structures cannot provide adequate wavefield information for inversion. Moreover, the uneven distribution of energy has a significantly negative influence on the waveform fitting between observed and calculated data during the process of FWI. Seismic waves with stronger energy have more contribution to the mismatch in the objective function than those with weak energy, even though the velocity contrasts are the same. Therefore, in this paper, we present an adaptive illumination compensation method to automatically weight the gradients in frequency-domain FWI based on seismic illumination analysis of 2D acoustic wave equation. This proposed method is able to compensate energy loss in the deep part of the model regarding the limited maximum offset and illumination blind zone in complex media. The calculation of the weighted factor depends on the illumination intensity of the corresponding location on the direction of seismic wave propagation. Reflection and transmission coefficients are used to control the process of adaptive compensation, which describe the energy distribution of seismic reflections and transmissions on both sides of an interface. The synthetic data tests show that our method can enhance both the FWI stability in poorly illuminated area and inversion accuracy in complex target zone.

THEORY

2D frequency-domain full waveform inversion

The 2D acoustic wave equation in the frequency domain (Tarantola, 1984; Han et al., 2013) is given by

$$(\omega^2/\kappa(x,z)u(x,z,\omega) + (\partial/\partial x)\{[1/\rho(x,z)][\partial u(x,z,\omega)/\partial x]\}$$

$$+ (\partial/\partial z)\{[1/\rho(x,z)][\partial u(x,z,\omega)/\partial z]\} = -s(x,z,\omega) \quad , \tag{1}$$

where ω is the circular frequency and $u(x,z,\omega)$ is the wavefield recorded at

coordinate (x,z). $\kappa(x,z)$, $\rho(x,z)$, and $s(x,z,\omega)$ denote the bulk modulus, density and source term, respectively. Here we use the optimized mixed-grid finite-difference method to simulate frequency-domain wave propagations (Hustedt et al., 2004). The inversion scheme is an inherent optimization problem based on the minimization of the data misfit, which is defined as the L_2-norm of the data residuals

$$C(m) = \tfrac{1}{2} \| u_{cal} - u_{obs} \|^2 \quad , \tag{2}$$

where u_{cal} and u_{obs} represent the observed and calculated data, respectively, and m means the inverted model parameter (P-wave velocity). Starting from a prior model m_0, the velocity model is updated by

$$m_{k+1} = m_k + \alpha_k \Delta m_k \quad , \tag{3}$$

where α_k is the step length at the k-th iteration of the inversion computed through a line search process ($k \geq 0$), and the model parameter perturbation Δm_k is written as

$$\Delta m_k = -Q_k \nabla_m C(m) \quad , \tag{4}$$

where Q_k is the L-BFGS (limited-memory Broyden-Fletcher-Goldfarb-Shanno) approximation of the inverse Hessian operator $H(m_k)^{-1} = \nabla^2 C(m_k)^{-1}$ (Byrd et al., 1995; Nocedal and Wright, 2006). Here, we use the L-BFGS method preconditioned by quasi-Newton operator to update velocity model.

In eq. (4), the gradient $\nabla_m C(m)$ of the misfit function with respect to the model parameter m is derived from the virtual source method (Pratt et al., 1998), which is represented by

$$\nabla_m C(m) = \sum_s \sum_r \mathrm{Re}\{\mathbf{u}^t [\partial \mathbf{S}^t / \partial m] \mathbf{r}_b\} \quad , \tag{5}$$

where $\mathbf{u}$ is the incident wavefield and $\mathbf{r}_b$ corresponds to the back-propagated residual wavefield. t denotes the transpose conjugate. The subscripts of the summary symbols, s and r, represent the source and receiver, respectively. $\mathbf{S}$ is the impedance matrix. This gradient can be calculated by the cross-correlation of the forward-propagated source wavefield and back-propagated residual wavefield.

However, when we use seismic data to recover the velocity variations in the deep and complex parts by waveform inversion, uneven energy distribution of seismic waves makes it difficult to achieve satisfactory results. First, near-surface waveforms dominate the data fitting in the inversion because

seismic reflection amplitudes decrease along with depth increasing. In other words, near-surface velocity updates have much more influence on the data fitting than the deep-part updates, especially in the limited seismic acquisition offsets. Second, poor-illuminated regions exist on the propagation direction of seismic waves because of the complexity of underground media. In the iterative process of waveform inversion, the better illumination area with high energy leads to a faster model update than the poor illumination area with low energy. To tackle the problem, we present one method in which we scale the velocity updates with weights according to the two-way illumination intensity.

The two-way wave equation illumination

Wave-equation illumination analysis needs to apply the imaging condition that calculates the cross-correlation between the downgoing wavefields D and upgoing wavefields U at the imaging location (Etgen, 1986). The imaging condition is expressed by

$$R(x,z) = \int D(x_s,x,z,t) \cdot U(x_r,x,z,t)dt \quad , \tag{6}$$

where R denotes the imaging at coordinate (x,z). The approximation of illumination energy at imaging point (x,z) for a pair of source x_s and receiver x_r can be obtained by replacing wavefields in eq. (6) with an estimation of the energy that reaches the imaging point (Alves et al.,2009). Mathematically it is represented by

$$\mathbf{I}(x,z) \cong \mathbf{G}_D(s,x,z) \cdot \mathbf{G}_U(r,x,z) \quad , \tag{7}$$

where $\mathbf{I}$ is the total illumination energy located at (x,z). $\mathbf{G}_D$ and $\mathbf{G}_U$ are the energy of downgoing and upgoing wavefields at the imaging point, respectively. Based on the principle of reciprocity, we replace the upgoing wavefields by the downward wavefields between source at the surface and the any subsurface imaging point. In this paper, we choose the finite difference numerical algorithm (Alford et al., 1974) to solve the two-way acoustic wave equation and calculate energy of wavefields. The sum of energy of source-receiver pairs (s,r) defined by the acquisition geometry is the two-way illumination intensity

$$\mathbf{I}(x,z) = \sum_s \sum_r [\int |G(x_s,x,z,t)|^2 |G(x_r,x,z,t)|^2 dt]^{1/2} \quad , \tag{8}$$

Adaptive energy compensation

To automatically balance the energy distribution of seismic waves, reflection and transmission coefficients are applied to control the procedure of

illumination based energy compensation. We now introduce the following assumptions: (1) The propagation directions of seismic waves are normal to the interface. (2) Each grid point (from the top to bottom) in our model represents a horizontal interface. We are able to judge whether there is a real interface with velocity contrast or not according to the velocity model. According to the two above mentioned assumptions, when the seismic waves encounter the interface between the n-th layer and the (n + 1)-th layer in the model, the expression for P-wave transmission and reflection coefficients (T and R) can be written as

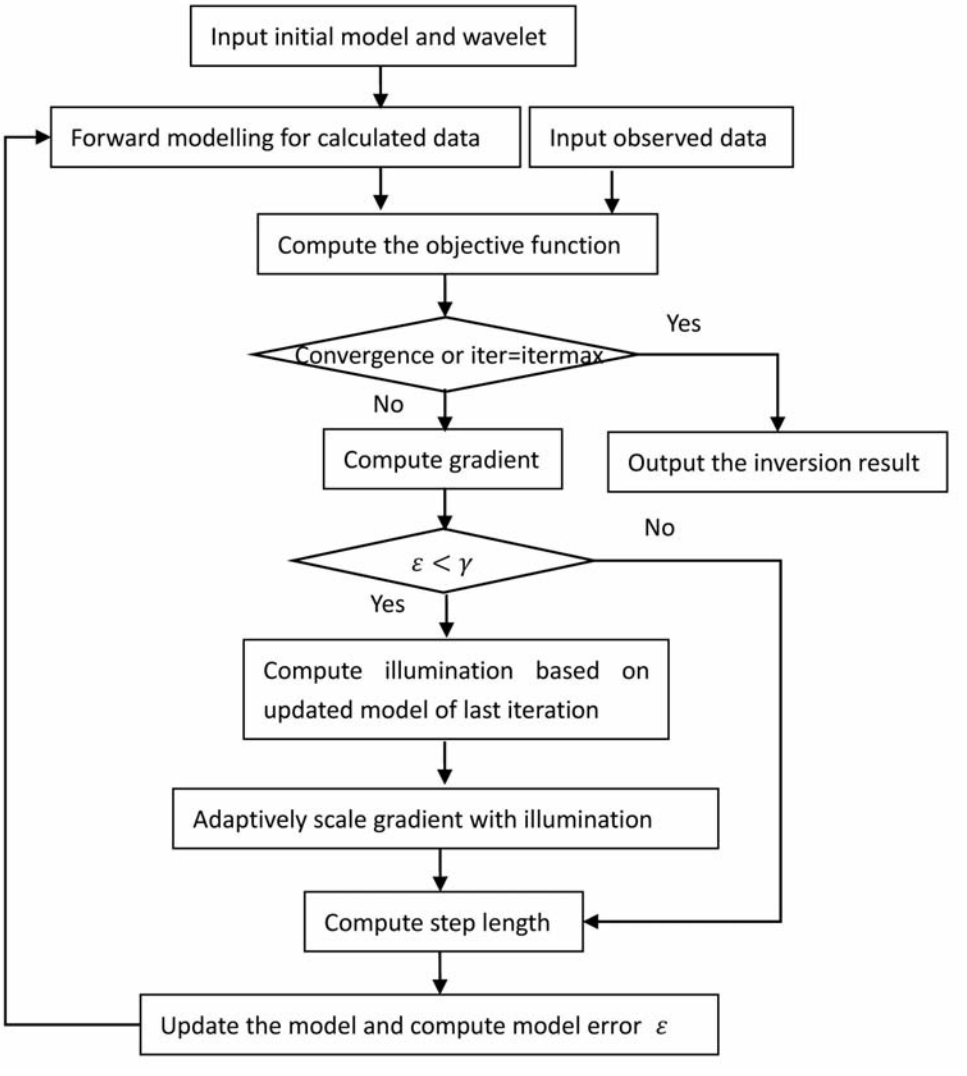

Fig. 1. Flowchart of the adaptive energy compensation for frequency-domain FWI based on seismic illumination analysis.

$$\begin{cases} T = 2\rho_n v_{p_n}/(\rho_{n+1} v_{p_{n+1}} + \rho_n v_{p_n}) \\ R = (\rho_{n+1} v_{p_{n+1}} - \rho_n v_{p_n})/(\rho_{n+1} v_{p_{n+1}} + \rho_n v_{p_n}) \end{cases}, \tag{9}$$

where ρ_n, v_{p_n} and ρ_{n+1}, $v_{p_{n+1}}$ are density, P-wave velocity of the n-th and the (n+1)-th layer, respectively. ρv_p denotes acoustic impedance. The case $T>1$ means that the acoustic impedance decreases from the upper side to the lower side of the interface. In this case, the transmission energy is stronger than reflection energy and we use the illumination intensity to down-weight the gradient. Whereas we use the illumination intensity to weight the gradient for the case $T < 1$ to balance the distribution of energy during inversion. The case $T = 1$ represents zero acoustic impedance contrast at the interface. For simplicity, the new model parameter perturbation $\Delta \mathbf{m}_k^{illum}$ at the k-th iteration for the FWI with adaptive illumination compensation is expressed as

$$\Delta \mathbf{m}_k^{illum}(x,z) = \begin{cases} \Delta \mathbf{m}_k(x,z) * \mathbf{I}(x,z) & T < 1 \\ \Delta \mathbf{m}_k(x,z) & T = 1 \\ \Delta \mathbf{m}_k(x,z) / \mathbf{I}(x,z) & T > 1 \end{cases}, \tag{10}$$

where $\mathbf{I}$ means the two-way illumination intensity. Fig. 1 shows the workflow of the adaptive energy compensation for frequency-domain FWI based on seismic illumination algorithm. There are three loops in the workflow (group frequencies, iterations and frequencies in one group). As the conventional FWI does, the relative error ε between inversion result and true model is calculated after each iteration. When the model error reaches a certain error expectancy γ ($\varepsilon \leq \gamma$), we start to calculate the seismic illumination intensity based on the updated model and adaptively compensate the gradient according to eq. (10) in the next iteration.

NUMERICAL TESTS

Model 1: Circular high-velocity anomaly model

A synthetic test is first carried out in a model with a circular high-velocity anomaly located in the middle (Fig. 2). The velocities of the anomaly and background are 3300 m/s and 3000 m/s, respectively. The size of the model is 10 × 5 km with a uniform 50 m grid interval. Regarding the simulation of seismic wave propagations, the perfectly matched layer (PML) is used to suppress unwanted reflections from edges of the model (Collino and Tsogka, 2001). We choose the Ricker wavelet as the source function which has peak frequency of 15 Hz and maximum frequency of about 40 Hz. Both shots and receivers are placed along the surface of this model. Total 200 shots with 50 m interval are simulated to obtain seismic profiles. We use 100 receivers to record seismic signal for each shot. The recording length of each shot is 4 s with 4 ms

sampling rate. When seismic survey line (maximum offset) is 5 km long, both receiver interval and minimum offset are set as 50 m. However, the receiver interval and the minimum offset are set as 100 m when the length of seismic survey line is 10 km.

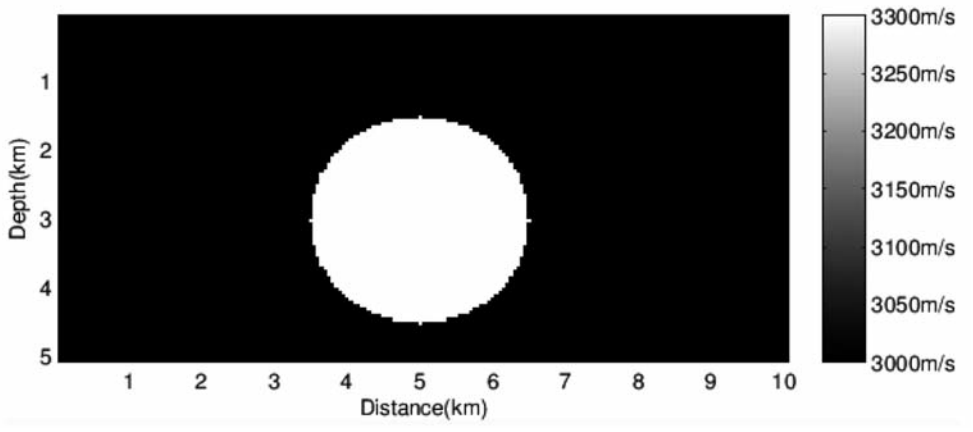

Fig. 2. The true velocity model with circular high-velocity anomaly.

For the implementation of full waveform inversion (FWI), the initial model is a homogeneous model with the background velocity, 3000 m/s. During the inversion, we use 10 frequency groups in the frequency band of 1-10 Hz based on our tests that we can get acceptable inversion results by 10 Hz maximum frequency. Fig. 3 shows the reconstructed velocity models by conventional FWI method in which 20 iterations of each frequency are carried out. One can easily observe that the inverted velocity imaging with 10 km maximum offset (Fig. 3a) matches the real model better than the inversion result using 5 km maximum offset (Fig. 3b). The possible reasons may include (1) the limited acquisition geometry makes it difficult to receive adequate information from deep structures, (2) the uneven distribution of energy adversely affects the inversion result, (3) near-surface waveforms dominate the data fitting in the inversion, and (4) the wide-angle reflection and refraction data only provide medium- to large-scale velocity information for inversion (Shipp and Singh, 2002). Hence a reduction in the maximum offset may limit the recovery of the lowest wavenumber media in the model, seriously affect the convergence of the inversion to a global minimum and prevent the recovery of the macro-model (Sirgue and Pratt, 2004).

To improve the quality of the inverted velocity imaging with short offset (5 km), we use the illumination intensity to adaptively balance the gradient of

FWI through seismic illumination analysis. Fig. 4a illustrates the two-way illumination intensity based on true model. The circular high-velocity anomaly causes the energy of seismic waves scattered beside itself. All of the inversion parameters are the same as conventional FWI. For the case of short offset, the inversion result with seismic illumination (Fig. 4b) is much better than the result from conventional FWI (Fig. 3b). To our surprise, compared with the conventional inversion result (Fig. 3a) with 10 km maximum offset, the inverted velocity in the anomaly zone in Fig. 4b is closer to the true model, which verifies the effectiveness of our new method.

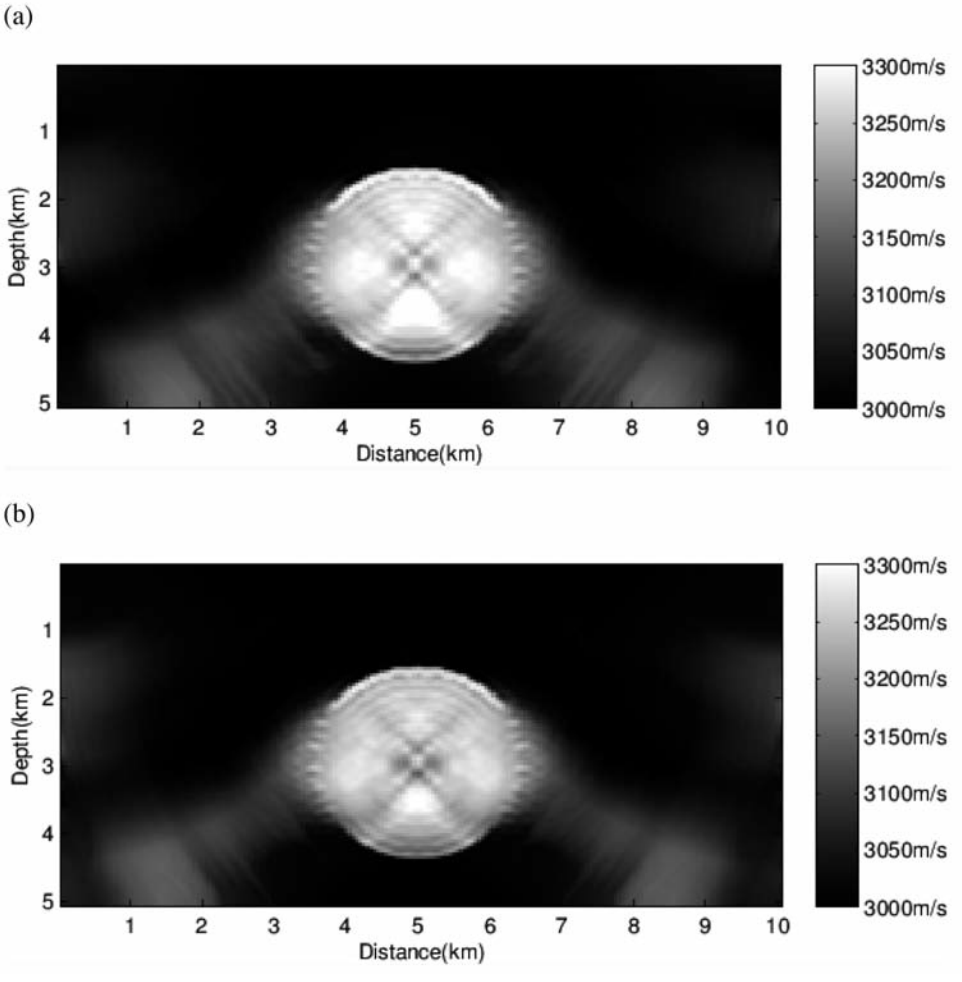

Fig. 3. The conventional inversion results with (a) 10 km maximum offset and (b) 5 km maximum offset.

In addition, we can observe that the inverted velocities on the lower left and right sides of the high-velocity anomaly are higher than the background velocity in the inversion results (Figs. 3a, 3b and 4b). The higher inverted velocities are also observed on the left and right sides of the model. The possible reason is that the sides of the circular anomaly behave like two vertical faults, which makes it difficult for FWI to reconstruct velocity due to strong downward energy reflection and scattering. This is confirmed by the seismic illumination intensity distribution (Fig. 4a).

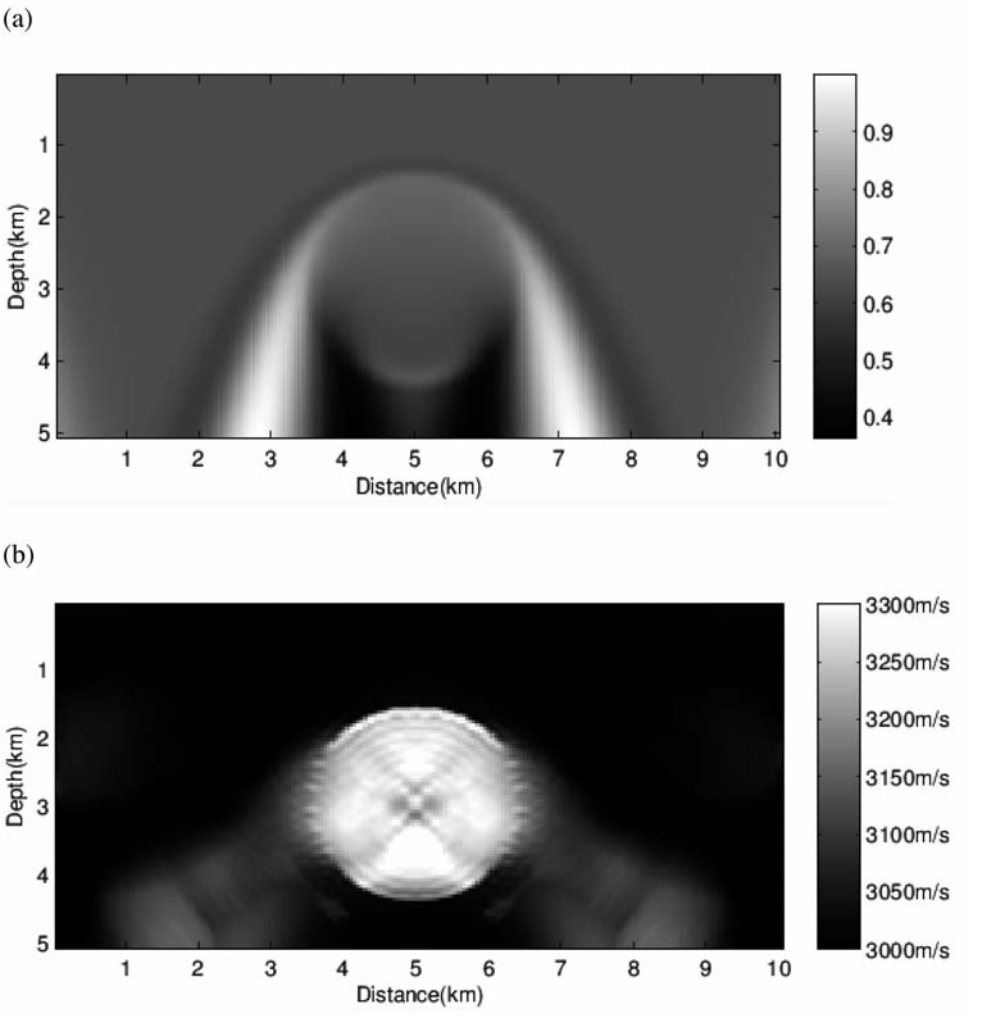

Fig. 4. (a) The two-way illumination intensity based on true model (Fig. 2). (b) The inversion result based on adaptive illumination compensation with 5 km maximum offset.

Model 2: Marmousi model

Here, we run the synthetic experiment on the Marmousi model to test our new algorithm. The size of the model is 10 × 3.12 km with a uniform 20 m grid interval (Fig. 5a). For the following FWI tests, the starting model (Fig. 5b) is obtained through smoothing the true model (Fig. 5a) using a 2D Gaussian filter. PML boundary conditions are also used in this model to simulate seismic wave propagation in unbounded media. In this test, seismic data are recorded by receivers up to 4 s with 2 ms sampling rate. In the acquisition system, both shots and receivers are spaced along the surface of this model. A total of 250 sources with 40 m interval are excited in turn with a Ricker wavelet with peak

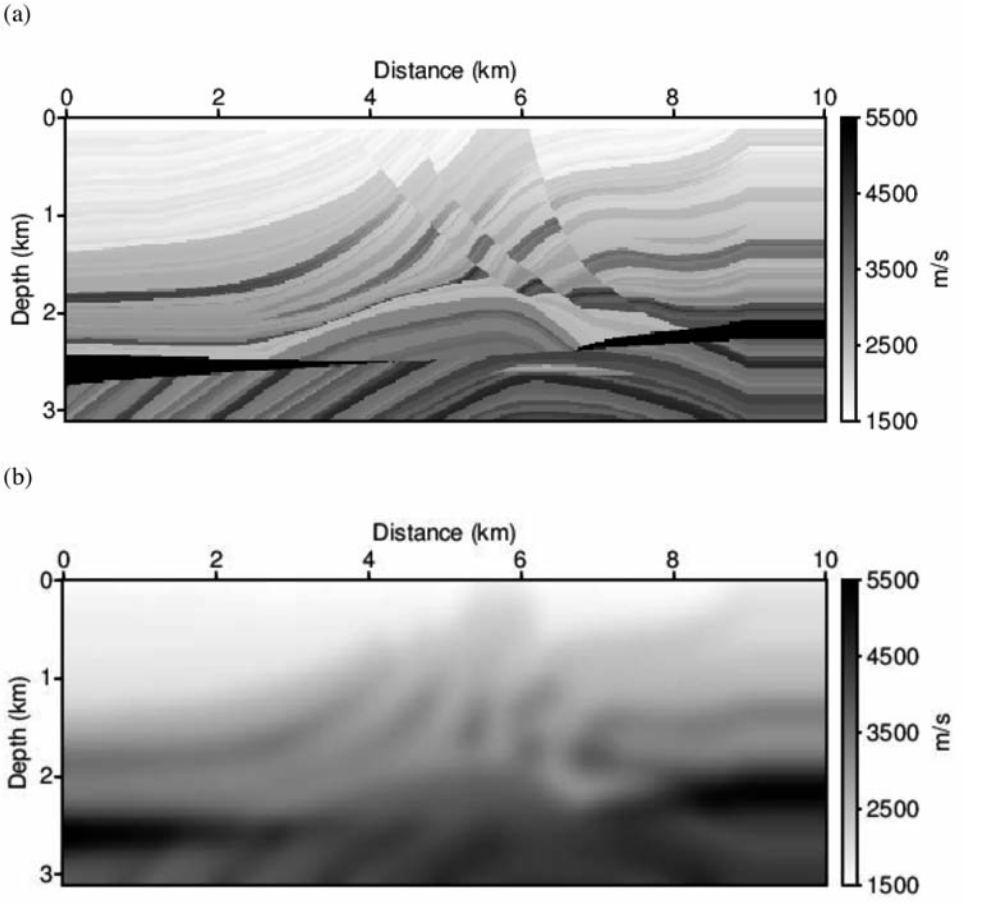

Fig. 5. (a) The Marmousi velocity model. (b) Initial model for FWI obtained from smoothing the true velocity model (a).

frequency of 30 Hz and maximum frequency of about 80 Hz. We also use 100 receivers to record seismic signal for each shot. When the survey line (maximum offset) is 10 km long, both receiver interval and the minimum offset are set as 100 m. However, the receiver interval and minimum offset are set as 20 m when the length of survey line is 2 km. Based on our tests of frequency selection, 15 frequency groups in the frequency band of 1.0-25.0 Hz are used during the inversions. The maximum iteration at each frequency is set as 30. All of the above parameters used in inversion (Fig. 6) are identical except the offset.

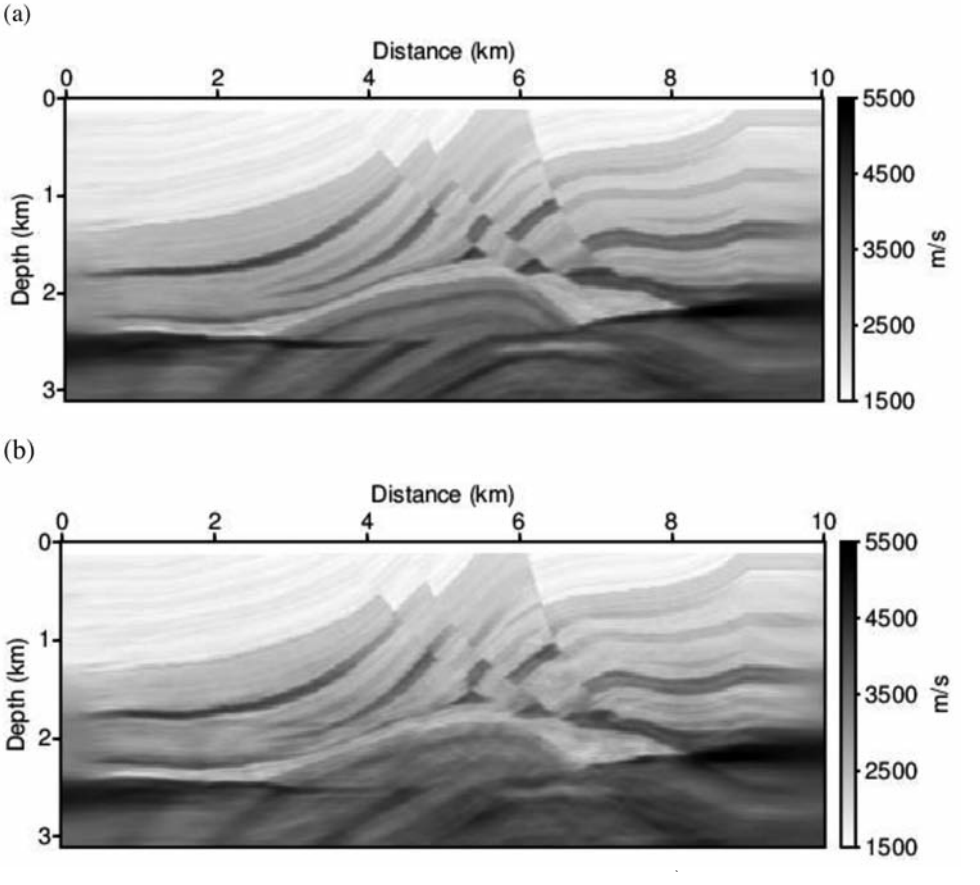

Fig. 6. The conventional inversion results with (a) 10 km maximum offset and (b) 2 km maximum offset.

The conventional waveform inversion results with 10 km maximum offset (Fig. 6a) provides a good match with the correct model, from large to intermediate wavelength scales. However, FWI with 2 km maximum offset does not work well as the inversion with 10 km maximum offset (Fig. 6b), especially in the deep region below the high velocity wedge. This shows that the limited maximum offset affects the quality of FWI. Fig. 7a shows the two-way illumination intensity. Fig. 7b shows the inversion result obtained by correcting the gradient adaptively using illumination compensation based on seismic acquisition with 2 km maximum offset. The inverted velocity imaging obtained by our new algorithm is significantly improved by comparing with the results from conventional FWI method.

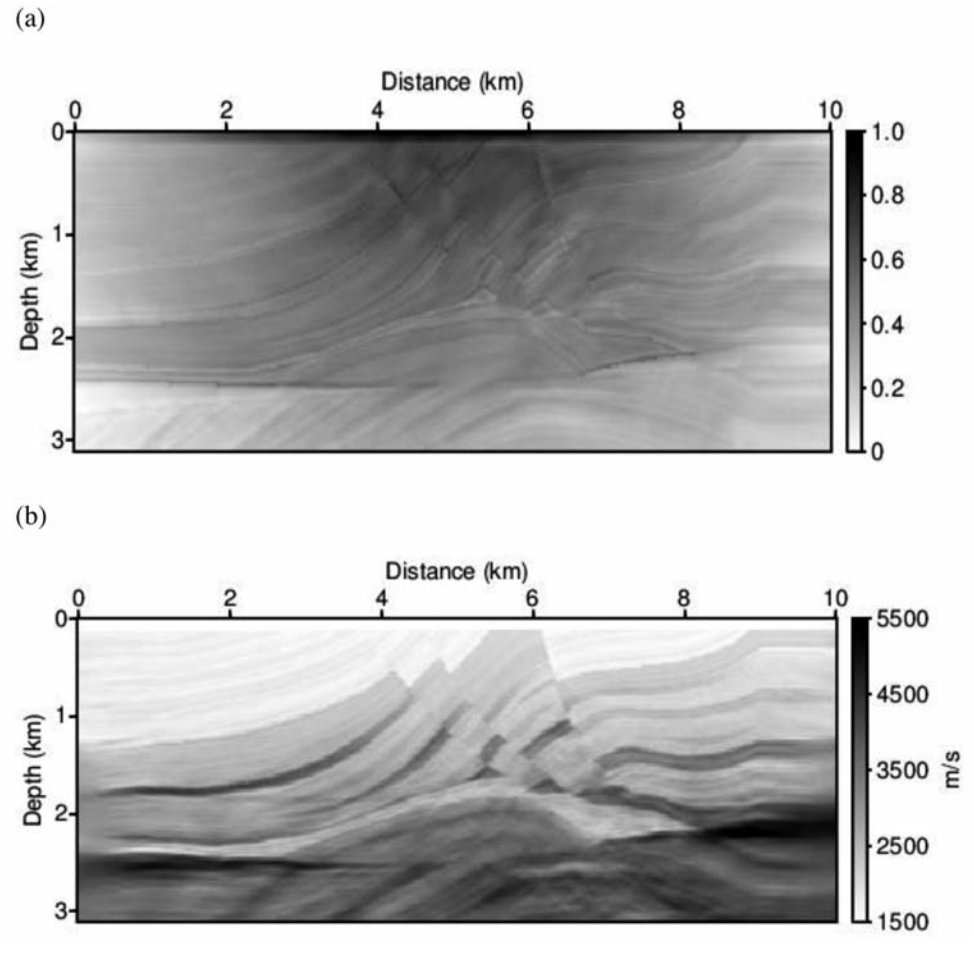

Fig. 7. (a) The two-way illumination intensity based on true model (Fig. 5a). (b) The inversion result based on adaptive illumination compensation with 2 km maximum offset.

CONCLUSION

The limited acquisition geometry and complex velocity structures leading to the inhomogeneous energy distribution of seismic wavefields have serious effect on imaging quality of full waveform inversion (FWI). In this paper, we have introduced a modified FWI algorithm based on adaptive illumination compensation to solve the problem of maximum offset restrictions. The synthetic tests have shown that the accuracy of inversion with adaptive illumination compensation has been improved compared with conventional inversion method. The proposed method can be further extended to elastic FWI.

ACKNOWLEDGMENT

This research is funded by the National Natural Science Foundation of China (No. 41374115) and the National High Technology Research and Development Program of China (863 Program, No. 2014AA06A605). The authors would also like to thank SunRise PetroSolutions Tech, Inc. for its partial support of this research. Some of the computing for this project was performed at the Tandy Supercomputing Center. The authors thank the anonymous reviewers for their constructive comments.

REFERENCES

Alford, M., Kelly, R. and Boore, M., 1974. Accuracy of finite difference modeling of the acoustic wave equation. Geophysics, 39: 834-842.

Alkhalifah, T. and Plessix, R., 2014. A recipe for practical full-waveform inversion in anisotropic media: An analytical parameter resolution study. Geophysics, 79: R91-R101.

Alkhalifah, T., 2015. Conditioning the full-waveform inversion gradient to welcome anisotropy. Geophysics, 80: R111-R122.

Alvès, C., Bulcão, A., Filho, S., Theodoro, E. and Santos, A., 2009. Target oriented approach for illumination analysis using wave equation via FDM. Expanded Abstr., 79th Ann. Internat. SEG Mtg., Houston: 181-185.

Bian, A., Zou, Z., Zhou, H. and Zhang, J., 2015. Evaluation of multi-scale full waveform inversion with marine vertical cable data. J. Earth Sci., 26: 481-486.

Boonyasiriwat, C., Valasek, P., Routh, P., Cao, W., Schuster, T. and Macy, B., 2009. An efficient multiscale method for time-domain waveform tomography. Geophysics, 74: WCC59-WCC68.

Borisov, D., Singh, S. and Fuji, N., 2015. An efficient method of 3-D elastic full waveform inversion using a finite-difference injection method for time-lapse imaging. Geophys. J. Internat., 202: 1908-1922.

Brossier, R., Operto, S. and Virieux, J., 2009. Seismic imaging of complex onshore structures by 2D elastic frequency-domain full-waveform inversion. Geophysics, 74: WCC105-WCC118.

Butzer, S., Kurzmann, A. and Bohlen, T., 2013. 3D elastic full-waveform inversion of small-scale heterogeneities in transmission geometry. Geophys. Prosp., 61: 1238-1251.

Bunks, C., Saleck, M., Zaleski, S. and Chavent, G., 1995. Multiscale seismic waveform inversion. Geophysics, 60: 1457-1473.

Byrd, H., Lu, P., Nocedal, J. and Zhu, C., 1995. A limited memory algorithm for bound constrained optimization. SIAM J. Scientif. Stat. Comput., 16: 1190-1208.

Chi, B., Dong, L. and Liu, Y., 2015. Correlation-based reflection full-waveform inversion. Geophysics, 80: R189-R202.

Collino, F. and Tsogka, C., 2001. Application of the perfectly matched absorbing layer model to the linear elastodynamic problem in anisotropic heterogeneous media. Geophysics, 66: 294-307.

Etgen, J., 1986. Prestack reverse time migration of shot profiles. Stanford Explor. Proj. Rep., 50: 151-169.

Fichtner, A., Trampert, J., Cupillard, P., Saygin, E., Taymaz, T., Capdeville, Y. and Villasenor, A., 2013. Multiscale full waveform inversion. Geophys. J. Internat., 194: 534-556.

Han, M., Han, L., Liu, C. and Chen, B., 2013. Frequency-domain auto-adapting full waveform inversion with blendedsource and frequency-group encoding. Appl. Geophys., 10: 41-52.

Hustedt, B., Operto, S. and Virieux, J., 2004. Mixed-grid and staggered-grid finite difference methods for frequency domain acoustic wave modelling. Geophys. J. Internat., 157: 1269-1296.

Mao, J., Wu, R. and Wang, B., 2012. Multiscale full waveform inversion using GPU. Expanded Abstr., 82nd Ann. Internat. SEG Mtg., Las Vegas: 1-7.

Nocedal, J. and Wright, J., 2006. Numerical Optimization, 2nd ed. Springer Science and Business Media, New York.

Pratt, G., Shin, C. and Hicks, J., 1998. Gauss-Newton and full Newton methods in frequency-space seismic waveform inversion. Geophys. J. Internat., 133: 341-362.

Pratt, G., 1999. Seismic waveform inversion in the frequency domain, Part 1: Theory and verification in a physical scale model. Geophysics, 64: 888-901.

Shipp, M. and Singh, C., 2002. Two-dimensional full wavefield inversion of wide-aperture marine seismic streamer data. Geophys. J. Internat., 151: 325-344.

Shin, C. and Cha, H., 2008. Waveform inversion in the Laplace domain. Geophys. J. Internat., 173: 922-931.

Shin, C., Koo, N., Cha, Y. and Park, K., 2010. Sequentially ordered single-frequency 2-D acoustic waveform inversion in the Laplace-Fourier domain. Geophys. J. Internat., 181: 935-950.

Shin, J., Ha, W., Jun, H., Min, D. and Shin, C., 2014. 3D Laplace-domain full waveform inversion using a single GPU card. Comput. Geosci., 67: 1-13.

Sirgue, L., Etgen, J. and Albertin, U., 2008. 3D frequency domain waveform inversion using time domain finite difference methods. Extended Abstr., 70th EAGE Conf., Rome: F022.

Sirgue, L. and Pratt, G., 2004. Efficient waveform inversion and imaging: a strategy for selecting temporal frequencies. Geophysics, 69: 231-248.

Son, M., Kim, Y., Shin, C. and Min, D., 2013. Time domain full waveform inversion using a time-window and Huber function norm. J. Seismic Explor., 22: 311-338.

Tarantola, A., 1984. Inversion of seismic reflection data in the acoustic approximation. Geophysics, 49: 1259-1266.

Vigh, D., Jiao, K., Watts, D. and Sun, D., 2014. Elastic full-waveform inversion application using multicomponent measurements of seismic data collection. Geophysics, 79: R63-R77.

Virieux, J. and Operto, S., 2009. An overview of full-waveform inversion in exploration geophysics. Geophysics, 74: WCC1-WCC26.

Wang, Y. and Rao, Y., 2009. Reflection seismic waveform tomography. J. Geophys. Res., 114: B03304.

Warner, M., Ratcliffe, A., Nangoo, T., Morgan, J., Umpleby, A., Shah, N., Vinje, V., Štekl, I., Guasch, L., Win, G., Conroy, G. and Bertrand, A., 2013. Anisotropic 3D full-waveform inversion. Geophysics, 78: R59-R80.

Xie, X., He, Y. and Li, P., 2013. Seismic illumination analysis and its applications in seismic survey design. Chin. J. Geophys., 56: 1568-1581 (in Chinese).

Xu, K. and McMechan, G.A., 2014.2D frequency-domain elastic full waveform inversion using time-domain modeling and a multistep-length gradient approach. Geophysics, 79: R41-R53.

Xu, S., Wang, D., Chen, F., Lambaré, G. and Zhang, Y., 2012. Inversion on reflected seismic wave. Expanded Abstr., 82nd Ann. Internat. SEG Mtg., Las Vegas: 1-7.

Xu, S., Wang, D., Chen, F., Zhang, Y. and Lambaré, G., 2012. Full waveform inversion for reflected seismic data. Extended Abstr., 74th EAGE Conf., Copenhagen: W024.

Yang, T., Shragge, J. and Sava, P., 2013, Illumination compensation for image-domain wavefield tomography. Geophysics, 78, U65-U76.

Zhou, H., Chen, S., Ren, H., Wang, H. and Chen, G., 2014. One-way wave equation least-squares migration based on illumination compensation. Chin. J. Geophys., 57: 726-738.

Zhu, X., McMechan, G.A. and Gong, T., 2014. Linearized AVA inversion of PP and PS reflections from low-velocity targets using Zoeppritz equations. J. Seismic Explor., 23: 313-339.